Wave front propagation failure in an inhomogeneous discrete Nagumo chain: Theory and experiments

S. Morfu*
Laboratoire d'Electronique, Informatique et Image (LE2i) (FRE.), CNRS 2309, Aile des Sciences de l'Ingénieur, Boîte Postale 47870, 21078 Dijon Cedex, France

V. I. Nekorkin†
Institute of Applied Physics of Russian Academy of Science, 46 Uljanov Street, 603600, Nizhny-Novgorod, Russia

J. M. Bilbault and P. Marquié
Laboratoire d'Electronique, Informatique et Image (LE2i), CNRS 2309, Aile des Sciences de l'Ingénieur, Boîte Postale 47870, 21078 Dijon Cedex, France

(Received 5 March 2002; published 22 October 2002)

The phenomenon of wave propagation failure in a discrete inhomogeneous Nagumo equation is investigated. It is found that the propagation failure occurs not only for small coupling coefficients but as well for an abrupt change of the interelement coupling. The investigation includes the study of the phase space of the system, numerical simulations, and real experiments with a nonlinear electrical lattice.

DOI: 10.1103/PhysRevE.66.046127 PACS number(s): 05.90.+m

I. INTRODUCTION

Systems composed of a large number of ordered in space interacting active subsystems, that is, active networks, arise in the study of many spatiotemporal phenomena in physics, chemistry, biophysics, technique, and so on. Take, for instance, arrays of Josephson junctions [1], arrays of coupled lasers [2], chains of coupled chemical reactors [3], nonlinear synchronization arrays [4], assemblies of biological oscillators [5], etc. The problems of pattern formation and propagation of nonlinear waves in active networks are widely investigated, as, for example, wave front dynamics in discrete bistable systems [6–11].

These systems are often modeled by the following well known discrete Nagumo equations:

$$\dot{V}_j = d(V_{j+1} - 2V_j + V_{j-1}) + f(V_j), \qquad j = 1,2,...,m-1 \tag{1}$$

with the dot accounting for the time derivative, j defining a space lattice point ($j \in \mathbf{Z}$) or discrete space coordinate, d being the coupling coefficient, while the cubic function $f(V)$ is given by

$$f(V) = V(V-1)(a-V), \quad 0 < a < 1.$$

The basic properties of Eq. (1) are the following:

(i) There exists a critical value of the coupling coefficient, $d = d^*(a)$, below which, i.e., $d \leqslant d^*(a)$ the wave fronts fail to propagate, this phenomenon being known as the wave front propagation failure [6,12,13].

(ii) The propagation of wave fronts (kinks and antikinks) is possible only for $d > d^*(a)$, the fronts emerging from a wide class of initial conditions. In particular, the initial conditions defining in $\{\mathbf{Z},\mathbf{R}\}$ kink-shape distributions belong to this class.

The existence of wave propagation failure is a characteristic feature of the discrete Nagumo equation, since this phenomenon does not occur in the continuous version of the Nagumo equation.

However, one might wonder how spatial inhomogeneities in a lattice described by a continuous or discrete Nagumo equation may influence the propagation failure conditions. Namely, in this paper, we consider an inhomogeneous Nagumo equation consisting in two homogeneous Nagumo subsystems connected at site m and described by the following set of coupled nonlinear equations:

$$\begin{aligned}
\frac{dV_j}{dt} &= d_1(V_{j+1} - 2V_j + V_{j-1}) + f(V_j), \qquad j = 1,2,...,m-1 \\
\frac{dV_m}{dt} &= d_1(V_{m-1} - V_m) + d_2(V_{m+1} - V_m) + f(V_m), \\
\frac{dV_j}{dt} &= d_2(V_{j+1} - 2V_j + V_{j-1}) + f(V_j), \\
& \qquad j = m+1, m+2, ..., N.
\end{aligned} \tag{2}$$

In the system (2), coupling coefficients between cells take two values d_1 and d_2, according to the index j defining a space point $j = 1,2,...,N$.

We note that in the special case $d_1 = d_2 = d$, the system (2) simply becomes an homogeneous discrete Nagumo equation (1) with the above described properties.

For the boundaries of the system (2), we impose zero-flux or Neumann conditions, that is, for $j = 1$ or $j = N$, respectively,

*Electronic address: smorfu@u-bourgogne.fr
†Electronic address: nekorkin@rf.unn.runnet.ru

$$V_1(t)=V_2(t) \quad \text{and} \quad V_N(t)=V_{N-1}(t). \tag{3}$$

Such model, for example, plays an important role in understanding the action potential propagation in inhomogeneous cardiac tissues [14,15] and in inhomogeneous nerve fibers [16–18]. Indeed, in myelinated nerve fibers the membrane activity is localized mostly in Ranvier nodes coupled by myelinated (passive) parts of the fiber. The inhomogeneities may be induced by variations of the diameter, changes of electrical properties, branching, and so on. Here, we will consider first the case of an inhomogeneous discrete Nagumo equation, then an inhomogeneous continuous one, both describing the propagation of excitation in a fiber with varying diameter. Note that our contribution based on phase planes analysis concerning the inhomogeneous continuous case, completes the study presented in Ref. [19].

The main result presented in this paper is the following: considering a kink propagating in the first Nagumo sublattice with coupling d_1, the propagation through the interface separating the two sublattices will be possible only if the coupling coefficient d_2 in the second sublattice stays in the range $[d^*_{\text{inf}}(d_1,a),d^*_{\text{sup}}(d_1,a)]$. The paper is organized as follows. Section II is devoted first to theoretical studies in a purely discrete inhomogeneous system, where specific (d_1,d_2) sets allow to exhibit propagation failure. We show then that the pinning of the front wave may also be possible even in a continuous inhomogeneous system. In this case d^*_{inf} vanishes to 0, and an analytical relation for $d^*_{\text{sup}}(d_1,a)$ is given. In Sec. III, we describe the experiments and present the results concerning the propagation failure in an inhomogeneous system, either in the discrete or in the continuous case. The shape of the pinned wave is given in a specific example of the latter case. In the final section, we give some concluding remarks.

II. PHASE SPACE ANALYSIS

In this section, we prove that the system (2), (3) [in the following, this system will be referred by Eq. (2)] has steady states that define steady patterns in the ''physical'' space $\{Z,R\}$, where the spatial profile corresponds to the kink distribution.

A. Gradient property of this system

Let us first prove the gradient property of this system. Introducing the function

$$G=\sum_{j=1}^{m-1}\left[\frac{d_1}{2}(V_{j+1}-V_j)^2-\int_0^{V_j}f(u)du\right] + \sum_{j=m}^{N}\left[\frac{d_2}{2}(V_{j+1}-V_j)^2-\int_0^{V_j}f(u)du\right], \tag{4}$$

it is simple to check that system (2) can be expressed as follows:

$$\frac{dV_j}{dt}=-\frac{\partial G}{\partial V_j}. \tag{5}$$

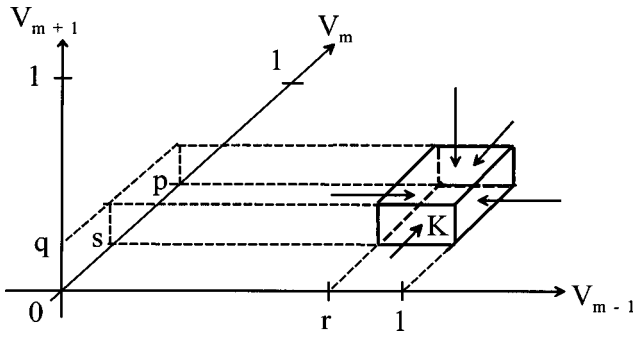

FIG. 1. Qualitative representation of region *K*.

Hence, it is a gradient one and only steady states can exist [20] in the phase space R^N of the system (2).

B. Absorbing region and stationary kink pattern

For determining the positions of the steady states of the system (2), let us introduce in phase space the region Ω such as $\Omega=\{\mathbf{V}:0\leqslant V_j\leqslant 1,\ j=1,2,...,N\}$.

By analogy with references [11,21], we can prove that all trajectories of system (2) with initial conditions outside of Ω tend to it. Consequently, all steady states of system (2) belong to region Ω. As a result, we can consider system (2) only in region Ω and hold that

$$0\leqslant V_j\leqslant 1 \quad \text{for} \quad t>0 \quad \text{and} \quad j=1,2,...N. \tag{6}$$

Let us now give more precisely invariant domains for the system (2). From now on, and for a sake of clarity we choose the parameter a to be smaller than 1/2 (the case $1/2<a<1$ could be straightforwardly deduced by symmetry properties).

Considering in phase space the following region (see Fig. 1):

$$K=\{\mathbf{V}:r\leqslant V_i\leqslant 1,\quad i=1,2,...,m-1\quad s\leqslant V_m\leqslant p,\quad 0\leqslant V_i\leqslant q,\quad i=m+1,...,N\}, \tag{7}$$

where r, s, p, and q are positive parameters between 0 and 1, we study the orientation of the vector field given by Eq. (2) on the boundary of region K, which will be denoted by ∂K.

First of all, we note that in the part of ∂K that is formed by planes $\{V_j=1\}$ and $\{V_j=0\}$, vector field (2) is oriented inward Ω since it attracts trajectories from outside, as seen previously. Considering then the remaining part of the boundary ∂K and using Eq. (5), we get from Eq. (2) for $i=1,2,...,m-2$:

$$\left.\frac{dV_i}{dt}\right|_{V_i=r}=f(r)+d_1(V_{i+1}-2r+V_{i-1})\geqslant f(r). \tag{8}$$

It follows from Eq. (7) and properties of the function $f(V)$ that inequality

$$\left.\frac{dV_j}{dt}\right|_{V_i=r}>0 \quad \text{for} \quad V_j\in\partial K,\forall j\neq i \tag{9}$$

is satisfied if parameter $r \in [a,1]$. Similarly, for the other equations of system (2), we find the following inequalities on boundary ∂K:

$$\left.\frac{dV_{m-1}}{dt}\right|_{V_{m-1}=r} = f(r) + d_1(V_{m-2} - 2r + V_m)$$
$$\geqslant f(r) - d_1 r + d_1 s,$$
$$\left.\frac{dV_m}{dt}\right|_{V_m=s} = f(s) + d_1(V_{m-1} - s) + d_2(V_{m+1} - s)$$
$$\geqslant f(s) - (d_1 + d_2)s + d_1 r,$$
$$\left.\frac{dV_m}{dt}\right|_{V_m=p} = f(p) - (d_1 + d_2)p + d_1 V_{m-1} + d_2 V_{m+1}$$
$$\leqslant f(p) - (d_1 + d_2)p + d_1 + d_2 q,$$
$$\left.\frac{dV_{m+1}}{dt}\right|_{V_{m+1}=q} = f(q) + d_2(V_m - 2q + V_{m+2})$$
$$\leqslant f(q) - d_2 q + d_2 p,$$
$$\left.\frac{dV_i}{dt}\right|_{V_i=q} = f(q) + d_2(V_{i-1} - 2q + V_{i+1}) \leqslant f(q)$$
$$\text{for} \quad i = m+2,...,N. \quad (10)$$

It is clear that, for $V_j \in \partial K (j = 1,2,...,N)$, the following inequalities:

$$\left.\frac{dV_{m-1}}{dt}\right|_{V_{m-1}=r} > 0, \quad \left.\frac{dV_m}{dt}\right|_{V_m=s} > 0, \quad \left.\frac{dV_m}{dt}\right|_{V_m=p} < 0,$$
$$\left.\frac{dV_{m+1}}{dt}\right|_{V_{m+1}=q} < 0, \quad \left.\frac{dV_i}{dt}\right|_{V_i=q} < 0, \quad i = m+2,...,N \quad (11)$$

will be satisfied provided that r, p, q, and s obey the following conditions:

$$a < r < 1, \quad 0 < q < a, \quad 0 \leqslant s < p \leqslant 1,$$
$$f(s) - (d_1 + d_2)s + d_1 r > 0,$$
$$f(p) - (d_1 + d_2)p + d_1 + d_2 q < 0, \quad (12)$$
$$f(q) - d_2 q + d_2 p < 0.$$

Taking into account the properties of the function $f(V)$, we find that, in the case $0 < a < 1/2$, inequalities (12) are satisfied at least for the following region of parameters:

$$\left\{ d_1 > 0, \ d_2 \leqslant \frac{a^2}{4} \right\} \cup \left\{ d_1 \leqslant \frac{a^2}{4}, \ d_2 > 0 \right\}. \quad (13)$$

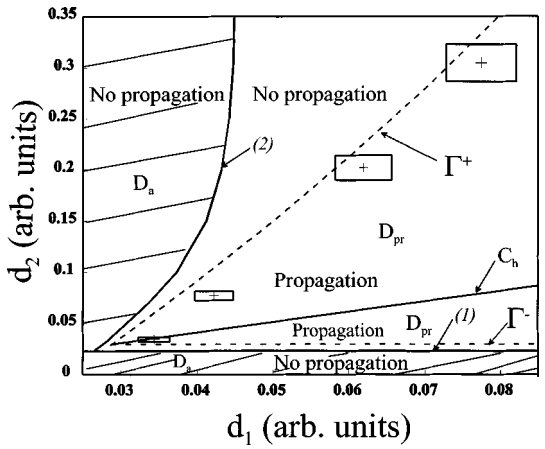

FIG. 2. Partition of the plane (d_1, d_2) for fixed a. Curves (1) and (2) are estimations of, respectively, d^*_{inf} and d^*_{sup} according to numerical resolution of Eqs. (12) and (13), providing the sufficient conditions: if $d_2 > d^*_{\text{sup}}$ or $d_2 < d^*_{\text{inf}}$, propagation fails. The region delimited by curves (1) and (2) is called D_a in the text. On the other hand, C_h corresponds to the homogeneous case $d_1 = d_2 > d^*(a)$. Then, the dotted lines correspond to a simulation of system (1) using a fourth-order Runge-Kutta algorithm with an integration time step 0.001, while the crosses correspond to experimental results obtained with the nonlinear electrical lattice. The parameters are $a = 0.3$, $N = 48$, $m = 24$.

For fixed a, the inequalities (13) define some region in the plane (d_1, d_2). However, this region can be extended more exactly thanks to numerical solution of inequalities (12) (see Fig. 2).

For these parameter values, region K exists in phase space, and the vector field on ∂K is oriented inwards, as shown by the qualitative view in phase space of Fig. 1. Since the system (2) has only steady states in phase space, we can conclude that region K keeps at least one of the stable steady states. Taking into account the spatial construction of the region K [see Eq. (7)] we find that this steady state in region K defines a steady kink-shape pattern.

Let us denote by D_a the region in the parameters space of the system (1.2) defined by the inequalities (12). Then numerical resolution of inequalities (12) demarcates by solid lines an hatched region D_a in the (d_1, d_2) plane of Fig. 2 for fixed a. Note that the region D_a is an estimation, corresponding to sufficient but not necessary conditions, of critical values of (d_1, d_2), allowing the pinning of wave fronts. Moreover, for any parameter (d_1, d_2) taken in region D_a, inequalities (12) are satisfied, that is, the wave front cannot propagate. On the other hand, in the parameter space of the system (1.2), there exists the set $\{d_1 = d_2, 0 < a < 1\}$ whose points are associated with the homogeneous Nagumo equation. Therefore, in this case, wave fronts propagation is possible if the parameters of the system (1.2) are taken from the line $C_h = \{d_2 = d_1 > d^*(a), 0 < a < 1/2\}$ (see the Introduction). Changing the parameters from C_h to D_a, we find that a surface Γ exists in the parameter space of the system (1.2) that determines the region of front propagation and its failure. The surface Γ has been obtained numerically with a direct simulation of system (1.2). On the plane (d_1, d_2) it

appears as two curves $\Gamma^+=\{d_2=d^*_{\rm sup}(d_1,a)\}$ and $\Gamma^-=\{d_2=d^*_{\rm inf}(d_1,a)\}$ originated from the common point $d_2=d_1=d^*(a)$ (see dashed curves in Fig. 2). Note that the curve Γ^- is close to the line $d_2=a^2/4$ and the region where the propagation is possible is restricted between Γ^- and Γ^+. We denote this region by D_{pr} (see Fig. 2).

C. The "nature" of the phenomenon

Let us consider the dynamics of the system (2) for the parameters taken from D_a. In this case, besides the spatio-homogeneous states $\{V_j=0\}$ and $\{V_j=1\}$, $j=1,2,...,N$, there also exists at least one spatially inhomogeneous steady state from region *K*. This inhomogeneous state attracts at least those initial distributions $V_j(0)$ that are located in the region *K*. This class of initial conditions in $\{\mathbf{Z},\mathbf{R}\}$ has a kink shape. Therefore, at variance with the homogeneous case [Eq. (1)] when such distributions evolve [see the point (ii) in the Introduction] to a traveling wave front (kink), in the inhomogeneous Eqs. (2) the wave front is not systematically established from such initial conditions. Namely, for parameters taken outside D_{pr}, wave front propagation failure takes place.

Note that propagation failure exists not only for small enough coupling strength between cells, but also when this coupling strength is large enough, which can be considered as a paradoxical result, because in this case the homogeneous Nagumo equation permits the front propagation. In fact, the system (2) consists of two parts, namely, two homogeneous Nagumo subsystems, which have connections in point $j=m$. Therefore, when at least one of these two subsystems is in propagation failure conditions, since its coupling coefficient is too small, the whole system demonstrates also propagation failure, and the coupling coefficient of the other subsystem has no importance. If both coupling coefficients d_1 and d_2 are large enough, each of single subsystem is free of propagation failure. Consequently, in this case, propagation failure in the whole system (2) is associated with a new reason, related with inhomogeneity of system (2).

It is well known that for large values of coupling coefficient between cells, discrete reaction-diffusion systems can be described by respective continuous equations to a high accuracy. In fact, it denotes that we found propagation failure even in the continuous case of system (2). We will now consider this case in some details.

D. Continuous limit

Let us define $x=x_0$ as the spatial coordinate corresponding to interface point $j=m$. To describe the system (1.2) in a continuous limit, let us change the spatial coordinate *j* to a continuous variable $x=j\delta$ with δ being the spatial lattice parameter of the discrete chain. Let us assume that the characteristic spatial scale of the kink-profile steady state is significantly larger than the spatial lattice parameter δ. Then we can transform variables as follows:

$$V_j(t)\to V(x,t),$$

$$V_{j-1}(t)\to V(x-\delta,t)=V(x,t)-\delta\frac{\partial V}{\partial x}+\frac{1}{2}\delta^2\frac{\partial^2 V}{\partial x^2}+\cdots, \tag{14}$$

$$V_{j+1}(t)\to V(x+\delta,t)=V(x,t)+\delta\frac{\partial V}{\partial x}+\frac{1}{2}\delta^2\frac{\partial^2 V}{\partial x^2}+\cdots.$$

Substituting Eq. (14) into the system (2) and neglecting the higher-order terms, we obtain the following system:

$$\begin{aligned}\frac{\partial V}{\partial t}&=f(V)+d_1\delta^2\frac{\partial^2 V}{\partial x^2}, \quad \text{if } x<x_0,\\ \frac{\partial V}{\partial t}&=f(V)+d_2\delta^2\frac{\partial^2 V}{\partial x^2}, \quad \text{if } x>x_0,\end{aligned} \tag{15}$$

with boundary conditions at the interface $x=x_0$

$$\begin{aligned}\left.\frac{\partial V}{\partial t}\right|_{x=x_0}=&d_1\left(-\delta\left.\frac{\partial V}{\partial x}\right|_{x=x_0^-}+\frac{1}{2}\left.\frac{\partial^2 V}{\partial x^2}\right|_{x=x_0^-}\right)\\ &+d_2\left(\delta\left.\frac{\partial V}{\partial x}\right|_{x=x_0^+}+\frac{1}{2}\left.\frac{\partial^2 V}{\partial x^2}\right|_{x=x_0^+}\right)+f(V_{\rm int}),\end{aligned} \tag{16}$$

where $x_0^{\pm}$ account for *x* values to the left and to the right sides, respectively, at $x=x_0$. We suppose that the variable *V* is continuous on *x*, that is $V(x_0^-)=V(x_0^+)=V_{\rm int}$. Then, using Eq. (15) for steady states, we have

$$\begin{aligned}d_1\delta^2\left.\frac{\partial^2 V}{\partial x^2}\right|_{x=x_0^-}&=-f(V(x_0^-))=-f(V_{\rm int}),\\ d_2\delta^2\left.\frac{\partial^2 V}{\partial x^2}\right|_{x=x_0^+}&=-f(V(x_0^+))=-f(V_{\rm int}).\end{aligned} \tag{17}$$

Using Eqs. (16) and (17) we obtain the boundary conditions

$$\begin{aligned}V|_{x=x_0^-}&=V|_{x=x_0^+},\\ d_1\left.\frac{\partial V}{\partial x}\right|_{x=x_0^-}&=d_2\left.\frac{\partial V}{\partial x}\right|_{x=x_0^+}.\end{aligned} \tag{18}$$

Note, that the boundary conditions (18) are typical for continuous inhomogeneous systems (see, for example, Eq. [16]). The steady states of the system (15) are determined by the following set of equations:

$$\begin{aligned}\frac{dV}{dx}&=U, \quad \delta^2 d_1\frac{dU}{dx}=-f(V), \quad \text{if } x<x_0,\\ \frac{dV}{dx}&=U, \quad \delta^2 d_2\frac{dU}{dx}=-f(V), \quad \text{if } x>x_0,\end{aligned} \tag{19}$$

where the variable *V* satisfies the conditions (18).

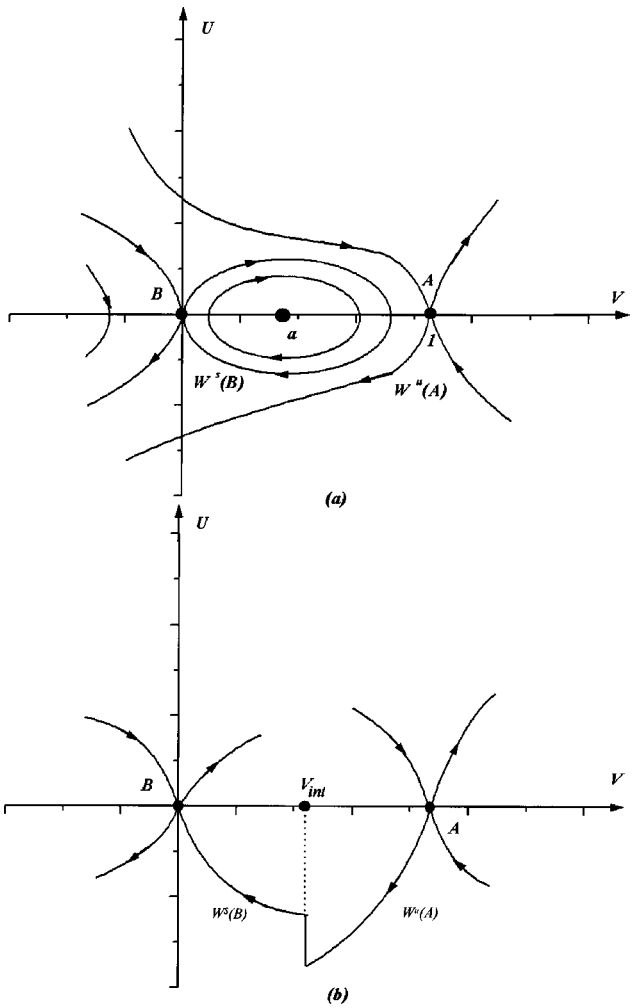

FIG. 3. (a) Phase portrait of system (19) when $d_1=d_2$; (b) Phase portrait of system (19) for $d_1\neq d_2$.

Let us look for a heteroclinic solution of this system, exhibiting steady states for a kink profile. When $d_1=d_2$ and for $a<1/2$, system (19) has the phase portrait presented in Fig. 3(a). In this case, each part of the system (19) does not possess any heteroclinic trajectory.

However, taking into account inhomogeneity in x_0 lets appear heteroclinic trajectories in system (19). Looking then for heteroclinic trajectories connecting the saddles $A(1,0)$ and $B(0,0)$, and the separatrix $W^u(A)$ and $W^s(B)$ located on the phase plane [Fig. 3(b)], we have to find which parameters allow to satisfy conditions (18).

Namely, $W^u(A)$ being the unstable separatrix of saddle A, standard calculations lead to

$$\delta^2 d_1\frac{U^2}{2}+\int_a^V f(\eta)d\eta=\int_a^1 f(\eta)d\eta. \tag{20}$$

By replacing $f(\eta)$ by its expression, we obtain straightforwardly the equation of $W^u(A)$, for $x<x_0$, and similarly for the stable separatrix of saddle B $W^s(B)$, when $x>x_0$:

$$U=-\frac{1-V}{\delta}\sqrt{\frac{3V^2+(1-2a)(2V+1)}{6d_1}} \quad \text{if } x<x_0,$$

$$U=-\frac{V}{\delta}\sqrt{\frac{3V^2-4(1+a)V+6a}{6d_2}} \quad \text{if } x>x_0. \tag{21}$$

Taking $0<V_{\rm int}<1$ and putting Eq. (21) in Eq. (19), we obtain the following conditions for which the steady state of the kink-profile exists in system (15) with boundary conditions (18):

$$d_2=k(V_{\rm int})d_1, \tag{22}$$

where

$$k(V_{\rm int})=1+\frac{1-2a}{V_{\rm int}^2[3V_{\rm int}^2-4(1+a)V_{\rm int}+6a]}. \tag{23}$$

Consequently, for each value of $V_{\rm int}$ in [0, 1] at the interface $x=x_0$, there exists a unique steady state of kink profile, if d_1 and d_2 are related by Eq. (22). Moreover, integrating Eqs. (21) with the boundary conditions $V(-\infty)=0$, $V(+\infty)=1$, and $V_{x_0}^-=V_{x_0}^+=V_{\rm int}$, the profile of this kink wave can be analytically expressed for each point of (d_1,d_2) plane satisfying Eq. (22). Furthermore, it is easy to show that $k(V_{\rm int})$ takes its minimum for all $V_{\rm int}\in[0,1]$ in $V_{\rm int}=a$, that is, $k(a)<k(V_{\rm int})$ for all $V_{\rm int}\neq a$. Hence, in the continuous limit the curve Γ^+ is given by

$$d_{\rm sup}^*=\frac{(1-a)^3(1+a)}{a^3(2-a)}d_1, \tag{24}$$

and corresponds specifically to the case $V_{\rm int}=a$.

Note that Eq. (24) requires large enough values of the coefficients d_1 and d_2 to be in the continuous approximation (15).

In Fig. 4, the region of existence of stationary kinks is presented for $a=0.44$. The comparison between the theoretical calculation [continuous line, Eq. (24)] and numerical simulations (dotted line) shows a good agreement for large enough d_1 and d_2, that is, when the continuum approximation is valid.

Note that we choose here $a=0.44$ to have d_1 and d_2 of similar size, then both homogeneous Nagumo subsystems satisfy the continuum approximation. In fact, as shown by Fig. 5, the slope $k(a)$ of the straight line given by Eq. (24), decreases very fast when a varies from 0 to 1/2. Thus, d_1 and d_2 have similar size only if $0.4<a<0.5$.

Finally, for any point satisfying Eq. (24), calculations of the stationary kink profile can be easily achieved, as $V_{\rm int}=a$.

It is straightforwardly given by

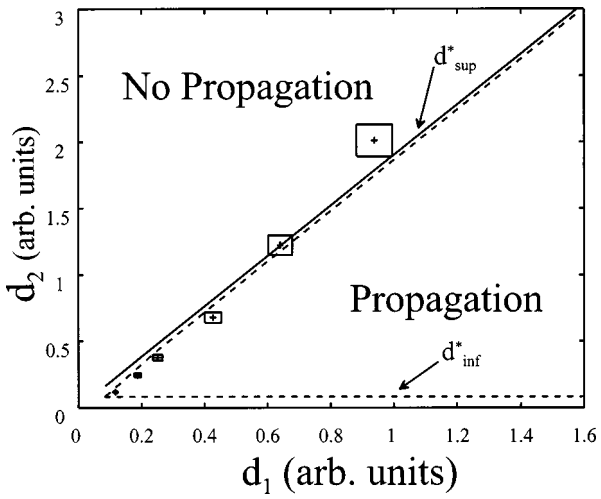

FIG. 4. Partition of the plane (d_1,d_2) in the continuous limit. The experimental results are presented by crosses with their uncertainties, while the solid lines are obtained by Eqs. (24) and (13). In addition, numerical simulations of system (1.2) appear in dashed line. The threshold a is set to 0.44.

$$x = x_0 + \delta\sqrt{\frac{d_1}{1-a}} \times\left[\operatorname{arctanh}\left(\sqrt{\frac{2}{3(1-a)}}\,\frac{2a-1-2V+aV}{\sqrt{3V^2+(1-2a)(1+2V)}}\right) + \operatorname{arctanh}\left(\sqrt{\frac{2(1+a)}{3}}\right)\right] \quad \text{if } x \leqslant x_0, \tag{25}$$

$$x = x_0 + \delta\sqrt{\frac{d^*_{\mathrm{sup}}}{a}}\left[\operatorname{arctanh}\left(\sqrt{\frac{2}{3a}}\,\frac{3a-aV-V}{\sqrt{3V^2-4V-4aV+6a}}\right) - \operatorname{arctanh}\left(\sqrt{\frac{2(2-a)}{3}}\right)\right] \quad \text{if } x \geqslant x_0$$

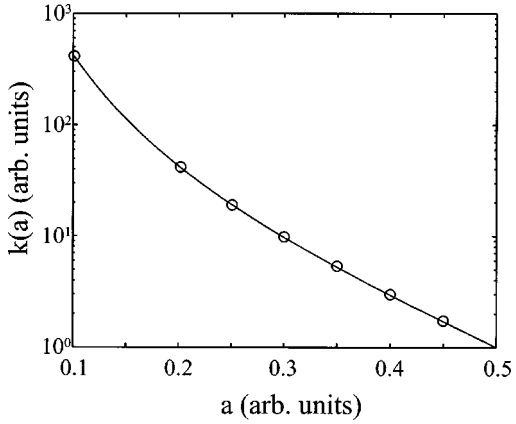

FIG. 5. Slope of the curves $d^*_{\mathrm{sup}} = k(a)d_1$. The solid line represents the slope coefficients obtained by Eq. (24) while the circles represent the simulation results.

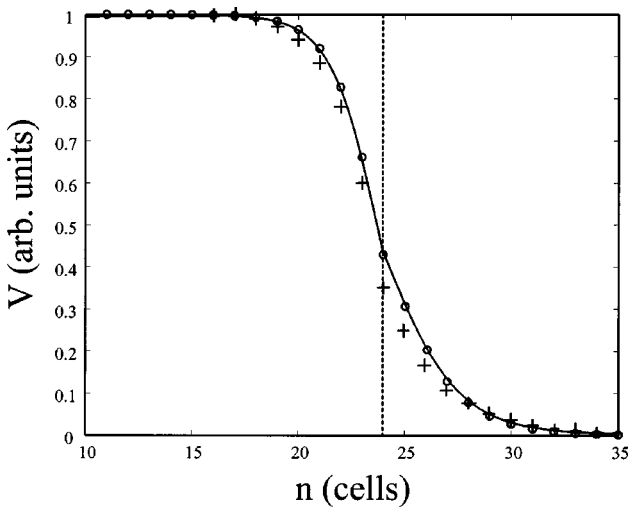

FIG. 6. Profile of the kink pinned at the interface. Parameters are $d_1 = 0.75 \pm 0.05$, $d_2 = d^*_{\mathrm{sup}} = 1.39 \pm 0.08$, $N = 48$, $m = 24$, $a = 0.44$. The solid line represents the profile obtained by Eq. (25), while the circles are obtained by numerical simulations and the crosses correspond to real experiments.

and is compared to simulation results in Fig. 6 in a specific example, when $a = 0.44$, $d_1 = 0.75$, and $d_2 = d^*_{\mathrm{sup}} = 1.388$.

III. ELECTRONIC EXPERIMENTS

Our experiments are carried out on an electrical chain, composed of $N = 48$ cells (see Fig. 7), including a linear capacitance C and a nonlinear resistor R_{NL}, whose current-voltage characteristic obeys the following cubic function $I_{NL} = (V/R_0)[1-(V/\alpha)][1-(V/\beta)]$. Here, α and β are the roots of the characteristic, and R_0 is a weighting resistor. Diffusion coupling is assured by linear resistors R_i, namely, $R_i = R_1$ for the $m = 24$ first cells, and $R_i = R_2$ for the 24 last ones.

Using Kirchhoff laws, we can model the voltage evolution by the following discrete equations set:

$$\frac{dV_i}{dt} = \frac{1}{R_1 C}(V_{i+1} - 2V_i + V_{i-1}) - \frac{V_i}{R_0 C}\left(1-\frac{V_i}{\alpha}\right)\left(1-\frac{V_i}{\beta}\right), \quad i = 1,2,\ldots,m-1$$

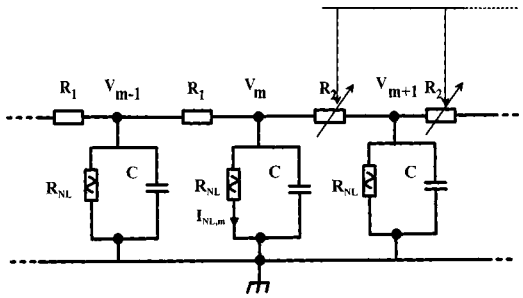

FIG. 7. Sketch of the real electrical lattice. Potentiometers R_2 are used to tune d_2, allowing experimental determination of d^*_{sup} and d^*_{inf}.

$$\frac{dV_m}{dt} = \frac{1}{R_1 C}(V_{m-1} - V_m) + \frac{1}{R_2 C}(V_{m+1} - V_m) - \frac{V_m}{R_0 C}\left(1 - \frac{V_m}{\alpha}\right)\left(1 - \frac{V_m}{\beta}\right),$$

$$\frac{dV_i}{dt} = \frac{1}{R_2 C}(V_{i+1} - 2V_i + V_{i-1}) - \frac{V_i}{R_0 C}\left(1 - \frac{V_i}{\alpha}\right)\left(1 - \frac{V_i}{\beta}\right), \quad i = m+1, m+2, ..., N. \tag{26}$$

In addition, the end of the chain satisfies Neumann boundary condition $V_N = V_{N-1}$.

After normalization, namely setting $v_i = V_i/\beta$, $d_1 = \alpha R_0/\beta R_1$, and $d_2 = \alpha R_0/\beta R_2$, Eqs. (26) appear to be an analog simulation of system (1.2).

As initial condition, voltage of each cell is at rest, $V_i = 0$, while we set the input voltage to the higher state, that is $V_1(t \geqslant 0) \equiv \beta$. The coupling coefficient d_1 being fixed, giving rise to a wave front along the chain, we analyze versus the coefficient d_2 either if the propagation of the front wave is possible or if it is pinned at the interface (mth cell).

As for the theoretical study, we will consider separately the purely discrete case and the continuous one.

1. Case of a purely discrete chain. We use potentiometers R_2 to obtain a precise measure of the critical values d^*_{sup} and d^*_{inf}. In the purely discrete case, the results referred by crosses in Fig. 2 are qualitatively in good agreement with numerical simulations of initial equations set (2). As one could expect, the first bisecting in the (d_1, d_2) plane, corresponding to homogeneous media, is located in the region where propagation is possible. Moreover, the first cross at the left bottom, located on the first bisecting is of great interest, since this experimental result corresponds, in a homogeneous media, to the measurement of the standard critical value d^* under which propagation fails [12].

2. Chain in the continuum approximation. The same chain is now used with smaller values of resistors R_1 and R_2, that is larger values of d_1 and d_2, to be in the continuous limit. Figure 4 shows that the experimental results are in good agreement with numerical simulations and theoretical prediction given by Eq. (24). The small observed discrepancy is mainly imputable to the experimental current-voltage characteristic that does not match exactly a cubic law. For the same reason, the experimental and the theoretical profiles of the kink pinned at the interface are slightly different in Fig. 6. The main feature is, however, verified, that is, there exists a maximal value of d_2, over which propagation in the inhomogeneous chain is not possible. Moreover, we note a good agreement between theoretical analysis, numerical simulations of Eq. (2) and experimental results.

IV. CONCLUDING REMARKS

In this paper, we have considered an inhomogeneous Nagumo system composed of two different homogeneous Nagumo subsystems. Namely, the coupling coefficient d_j is different in the two subsystems $d_j = d_1$ for $j \leqslant m$ and $d_j = d_2$ for $j > m$, m being the interface site. We have studied theoretically if a front wave (a kink) is able to propagate or fails to propagate in the discrete system, and we have shown the existence of a window $[d^*_{\text{inf}}, d^*_{\text{sup}}]$, for fixed a and d_1, allowing propagation. Outside this window, propagation is impossible. The existence of d^*_{inf} is related to the discreteness of the system; besides, if $d_2 = d_1$, we find again the standard results concerning propagation failure in an homogeneous case. On the other hand, the existence of d^*_{sup} is more surprising, and we wanted to study if this limit remains even in the continuous approximation.

In this approximation—larger d_1 and d_2 values—analytical calculations can be led farther, and confirm the existence of an upper limit of d_2, that is d^*_{sup}, for kink propagation. Moreover, analytical expression of d^*_{sup} is in good agreement with results of numerical simulations made with system (2) before any approximation. In addition, the kink profile, when $d_2 = d^*_{\text{sup}}$, is the same in theory and in numerical simulations. Then, the existence of d^*_{sup} is not related to the discreteness of the chain, but comes rather from continuity relations (18). Finally, our study is completed by experiments on an electrical chain consisting in two parts. For fixed d_1 and a, we change d_2 to measure d^*_{inf} and d^*_{sup}. Experimental results are in good qualitative agreement with theoretical predictions and simulations. A slight discrepancy is observed quantitatively, but it is due to the components uncertainties and to the experimental nonlinear current-voltage characteristic. The existence of d^*_{sup} extends Mornev's study [19] in the discrete case and is confirmed by experiments in the continuous one.

Moreover, recent studies of action potential propagation in inhomogeneous cardiac tissue [14,15] has also observed this phenomenon. Our theoretical and experimental study can be in fact useful in research concerning cardiac tissue or myelinated fibers or other domains in biology where homogeneity is not standard: in these cases, propagation failure can occur due to an inhomogeneous part of the system, independently of its discrete or continuous character.

ACKNOWLEDGMENTS

We would like to thank the Russian Foundation for Basic Research under Grant No. 00-02-16400 and Russian-French Grant No. 04610PA.

[1] A. V. Ustinov, Physica D **123**, 315 (1998).
[2] R. D. Li and T. Erneux, Phys. Rev. A **49**, 1301 (1994).
[3] V. Booth, T. Erneux, and J. P. Laplante, J. Phys. Chem. **98**, 6537 (1994).
[4] V. S. Afraimovich, V. I. Nekorkin, G. V. Osipov, and V. D. Shalfeev, *Stability, Structures and Chaos in Nonlinear Synchronization Networks* (World Scientific, Singapore, 1995).
[5] A. T. Winfree, *The Geometry of Biological Time*, 2nd ed.

(Springer-Verlag, Berlin, 1990).
[6] J. P. Keener, SIAM (Soc. Ind. Appl. Math.) J. Appl. Math. **47**, 556 (1987).
[7] B. Zinner, SIAM (Soc. Ind. Appl. Math.) J. Math. Anal. **22**, 1016 (1991).
[8] B. Zinner, J. Diff. Eqns. **96**, 1 (1992).
[9] J. P. Keener, Physica D **136**, 1 (2000).
[10] K. Kladko, I. Mitkov, and A. R. Bishop, Phys. Rev. Lett. **84**, 4505 (2000).
[11] V. I. Nekorkin, V. B. Kazantsev, S. Morfu, J.-M. Bilbault, and P. Marquié, Phys. Rev. E **64**, 036602 (2001).
[12] J. C. Comte, S. Morfu, and P. Marquié, Phys. Rev. E **64**, 027102 (2001).
[13] I. Mitkov, K. Kladko, and J. E. Pearson, Phys. Rev. Lett. **81**, 5453 (1998).
[14] Y. Wang and Y. Rudy, Am. J. Physiol. **278**, H1019 (2000).
[15] S. Morfu, J. C. Comte, P. Marquié, and J. M. Bilbault, Phys. Lett. A **294**, 304 (2002).
[16] J. Bell, Math. Biosci. **54**, 181 (1981).
[17] J. Bell and C. Cosner, Q. Appl. Math. **42**, 1 (1984).
[18] V. S. Markin, V. F. Pastushenko, and Y. A. Chizmadzhev, *Theory of Excitable Media* (Wiley, New York, 1987).
[19] O. A. Mornev, *Elements of the "Optics" of Autowaves*, *in Nonlinear Wave Processes in Excitable Media*, edited by A. V. Holden, M. Markus, and H. G. Othners (Plenum Press, New York, 1991), p. 111.
[20] P. Tu, *Dynamic Systems. An Introduction with Application in Economics and Biology* (Springer-Verlag, Berlin, 1994).
[21] V. I. Nekorkin, V. A. Makarov, V. B. Kazantsev, and M. G. Velarde, Physica D **100**, 330 (1997).